ATP7A Gene Addition to the Choroid Plexus Results in Long-term Rescue of the Lethal Copper Transport Defect in a Menkes Disease Mouse Model

Anthony Donsante[1], Ling Yi[1], Patricia M Zerfas[2], Lauren R Brinster[2], Patricia Sullivan[3], David S Goldstein[3], Joseph Prohaska[4], Jose A Centeno[5], Elisabeth Rushing[6] and Stephen G Kaler[1]

[1]Unit on Human Copper Metabolism, Molecular Medicine Program, Eunice Kennedy Shriver National Institute of Child Health and Human Development, National Institutes of Health, Bethesda, Maryland, USA; [2]Division of Veterinary Resources, Office of Research Services, National Institutes of Health, Bethesda, Maryland, USA; [3]Clinical Neurocardiology Section, National Institute of Neurological Disorders and Stroke, National Institutes of Health, Bethesda, Maryland, USA; [4]Department of Biochemistry and Molecular Biology, University of Minnesota Medical School, Duluth, Minnesota, USA; [5]Division of Biophysical Toxicology, U.S. Armed Forces Institute of Pathology, Washington, District of Columbia, USA; [6]Department of Neuropathology and Ophthalmic Pathology, U.S. Armed Forces Institute of Pathology, Washington, District of Columbia, USA

Menkes disease is a lethal infantile neurodegenerative disorder of copper metabolism caused by mutations in a P-type ATPase, ATP7A. Currently available treatment (daily subcutaneous copper injections) is not entirely effective in the majority of affected individuals. The mottled-brindled (*mo-br*) mouse recapitulates the Menkes phenotype, including abnormal copper transport to the brain owing to mutation in the murine homolog, *Atp7a*, and dies by 14 days of age. We documented that *mo-br* mice on C57BL/6 background were not rescued by peripheral copper administration, and used this model to evaluate brain-directed therapies. Neonatal *mo-br* mice received lateral ventricle injections of either adeno-associated virus serotype 5 (AAV5) harboring a reduced-size human ATP7A (rsATP7A) complementary DNA (cDNA), copper chloride, or both. AAV5-rsATP7A showed selective transduction of choroid plexus epithelia and AAV5-rsATP7A plus copper combination treatment rescued *mo-br* mice; 86% survived to weaning (21 days), median survival increased to 43 days, 37% lived beyond 100 days, and 22% survived to the study end point (300 days). This synergistic treatment effect correlated with increased brain copper levels, enhanced activity of dopamine-β-hydroxylase, a copper-dependent enzyme, and correction of brain pathology. Our findings provide the first definitive evidence that gene therapy may have clinical utility in the treatment of Menkes disease.

Received 8 March 2011; accepted 18 June 2011; published online 30 August 2011. doi:10.1038/mt.2011.143

INTRODUCTION

Menkes disease (MIM 309400) is an X-linked recessive disorder of copper metabolism caused by mutations in the copper-transporting P-type ATPase, ATP7A.[1–4] ATP7A has vital roles in absorption of copper across the intestinal mucosa and transport across the blood–brain and blood–cerebrospinal fluid barriers.[5–7] In addition to cellular export of copper, ATP7A conveys copper from the cytosol into the *trans*-Golgi network,[8] where it is packaged into copper-dependent enzymes undergoing maturation in the secretory pathway, including dopamine-β-hydroxylase, lysyl oxidase, peptidylglycine-α-amidating monooxygenase, and tyrosinase. ATP7A also appears critical for proper axonal development, synaptogenesis, and neuronal activation via *N*-methyl-D-aspartate receptor modulation.[9–12]

Even under ideal circumstances, ~75% of Menkes disease infants treated with subcutaneous copper injections show suboptimal clinical outcomes[13] and therefore alternative remedies are needed. Emerging molecular correlations indicate that Menkes disease infants with profound loss-of-function *ATP7A* mutations are particularly less likely to respond favorably to early copper treatment.[13,14] Since, we previously documented low copper levels in brain and cerebrospinal fluid of Menkes disease infants,[7] even after very early institution of copper injections,[6] we sought to evaluate novel brain-directed treatment strategies, including gene therapy. Such approaches could be relevant to Menkes disease patients with severe mutations for whom response to conventional treatment is predicted to be suboptimal. In addition, there are two allelic variants of Menkes disease, occipital horn syndrome and ATP7A-related distal motor neuropathy, for which gene transfer strategies may be appropriate.[15,16] There are no currently available treatments to ameliorate the connective tissue and peripheral nervous system abnormalities, respectively, that characterize these variants.

The mottled-brindled (*mo-br*) mouse provides a useful animal model of Menkes disease in which to evaluate brain-directed approaches preclinically. *Mo-br* mice (**Figure 1a**) have a 6 bp deletion in *Atp7a*, the murine homolog of *ATP7A*, resulting in a

Correspondence: *Stephen G Kaler, Unit on Human Copper Metabolism, Molecular Medicine Program, Eunice Kennedy Shriver National Institute of Child Health and Human Development, National Institutes of Health, Building 10; Room 10N313, 10 Center Drive MSC 1853, Bethesda, Maryland 20892-1853, USA. E-mail: kalers@mail.nih.gov*

mutant Atp7a protein lacking two highly conserved amino acids (Figure 1b).[17,18] Affected mice show decreased coat pigmentation, tremor, general inactivity, severely reduced copper levels in liver and brain, decreased copper enzyme activities, and death by 14 days of age.[19] We evaluated the clinical, biochemical, pathological, and neurobehavioral effects of brain-directed therapies in this model.

RESULTS

Characterization of the *mo-br* allele

Previous studies indicated that lifespan in *mo-br* mice (Figure 1a) was lengthened by intraperitoneal copper injections,[20] and that normal viability could be restored by a single injection administered on postnatal day 7.[21,22] The genetic background of mice in those experiments was not reported, however, and *Atp7a*$^{mo\text{-}br}$ was moved to The Jackson Laboratory's C57BL/6 background (http://

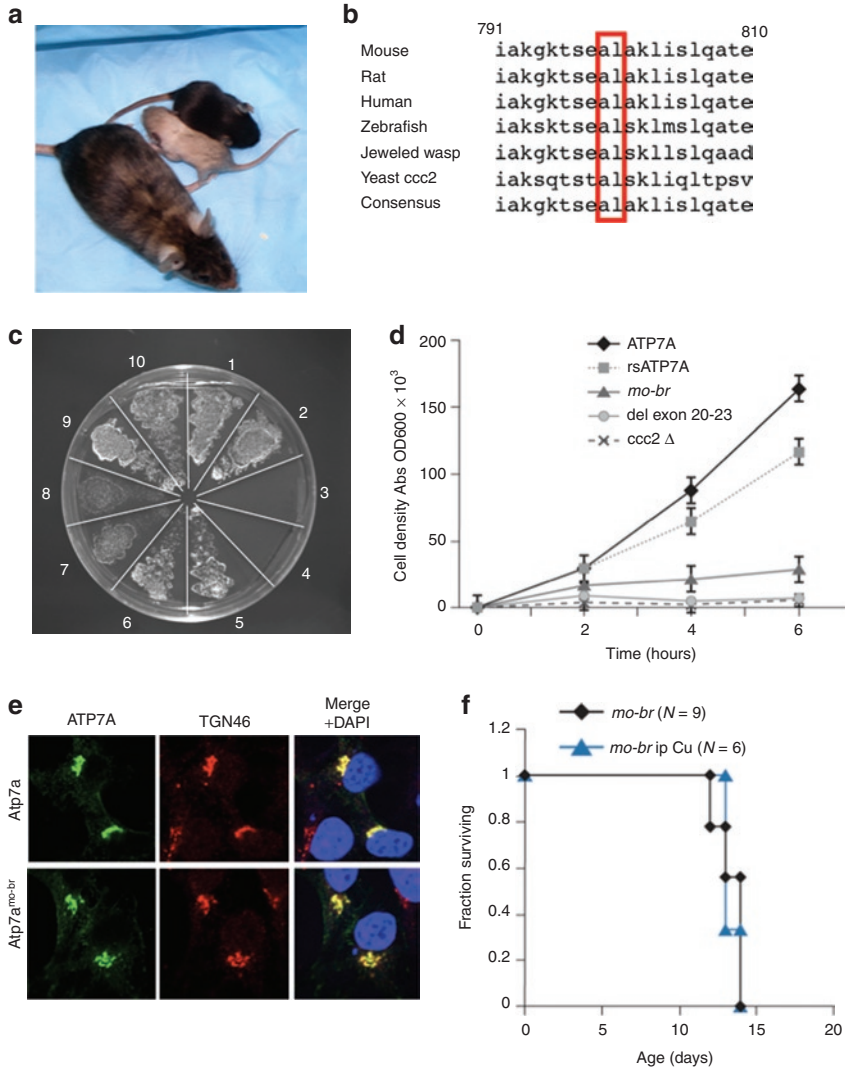

Figure 1 Characterization of C57BL/6-*Atp7a*$^{mo\text{-}br}$ mouse model of Menkes disease. (**a**) Mutant (gray coat color) and wild-type (black coat color) 12-day pups with a heterozygote female mother (mottled coat color). (**b**) Conservation among eukaryotic species of amino acid residues 799 (alanine) and 800 (leucine), which are deleted in *Atp7a*$^{mo\text{-}br}$. (**c**) On copper-deficient solid media, yeast transformation indicated partial complementation of the *S. cerevisiae* copper transport mutant, *ccc2*Δ, by *Atp7a*$^{mo\text{-}br}$. Plating pattern (clockwise from 12 O'clock) of the *S. cerevisiae* copper transport mutant *ccc2*Δ transformed with: wild-type human *ATP7A* (sections 1 and 2); an empty vector (sections 3 and 4); *rsATP7A* used as the adeno-associated virus serotype 5 (AAV5) transgene (sections 5 and 6); *Atp7a*$^{mo\text{-}br}$ (sections 7 and 8); and wild-type mouse *Atp7a* (sections 9 and 10). The *Atp7a*$^{mo\text{-}br}$ allele showed faint growth consistent with partial complementation. The *rsATP7A* allele restored growth nearly as well as either the wild type mouse or the wild type human copper ATPase. (**d**) Yeast complementation growth assay. Growth of various *ATP7A* alleles expressed in *ccc2*Δ, and cultured in copper-deficient media. The wild-type *ATP7A* allele complemented *ccc2*Δ efficiently, as did the *rsAP7A* used as the AAV5 transgene in brain-directed treatments of *mo-br* mice. The *rsAP7A* showed copper transport capacity ~80% compared to wild type in this growth assay. In contrast, the *Atp7a*$^{mo\text{-}br}$ allele, which lacks two highly conserved amino acids, showed <15% copper transport function compared to wild type. Transformation with an ATP7A allele harboring deletion of exons 20–23 (del ex20-23), included as a negative control, did not complement *ccc2*Δ. Mock-transformed *ccc2*Δ also failed to grow, as expected. (**e**) Intracellular localization of Venus-tagged *Atp7a* (upper row) and *Atp7a*$^{mo\text{-}br}$ (lower row) following transfection of human embryonic kidney-293 (HEK-293T) cells. Both alleles show *trans*-Golgi localization as noted by overlap of the ATP7A signal with TGN46, a *trans*-Golgi marker (merge + DAPI column). DAPI, 4′,6 diamidino-2-phenylindole, dihydrochloride nuclear counterstain. (**f**) Kaplan–Meier survival curve indicating failure of intraperitoneal (i.p.) copper chloride (dose = 10 µg/g body weight on postnatal day 7) to rescue *mo-br* males.

jaxmice.jax.org/strain/000664.html). More recently, we became aware that, on a mixed CBA/C3H background, this allele could be rescued by subcutaneous or intraperitoneal copper injections (J. Mercer, Deakin University, Burwood, Victoria, Australia, personal communication, 3 February 2009), suggesting an influence of genetic modifiers on response to systemic treatment.[23]

Given that *mo-br* mice on unknown and heterogeneous backgrounds had been rescued by peripheral copper treatment,[21,22] we suspected that Atp7a$^{mo\text{-}br}$ possessed partial copper transport capacity. To explore this, we characterized the mutation through several means. Yeast complementation assays showed weak cross-correction of the *Saccharomyces cerevisiae* copper transport knockout, *ccc2*Δ (**Figure 1c,d**). Transfection of human embryonic kidney-293 (HEK-293T) cells with Venus-tagged *Atp7a$^{mo\text{-}br}$* showed proper intracellular localization at the *trans*-Golgi network comparable to wild-type *Atp7a* (**Figure 1e**), whereas relocalization to the plasma membrane in response to copper was impaired (data not shown), confirming previous results.[18] Western blot analysis revealed normal size and quantity of the mutant protein in brain (data not shown), also confirming results from an earlier study.[18] Taken together, these findings indicate that *Atp7a$^{mo\text{-}br}$* drastically impairs, but may not eliminate, copper transport.

In the mice for our experiments, the *Atp7a$^{mo\text{-}br}$* allele was maintained on a homogenous C57BL/6 background, and intraperitoneal copper administration at doses reported previously by others[21,22] failed to extend lifespan (**Figure 1f**).

Brain-directed therapy in *mo-br* mice

We injected the lateral cerebral ventricles of neonatal *mo-br* C57BL/6 mice with either recombinant adeno-associated virus serotype 5 (AAV5) (**Figure 2a**) harboring a reduced-size complementary DNA (cDNA) of the human homolog, *ATP7A* (*rsATP7A*, **Figure 2b**), copper (as $CuCl_2$), or both. The cDNA was modified due to AAV packaging limits and included the final two of six *N*-terminal copper-binding motifs. For transgene detection purposes, a 6xHis-tag was inserted after the initial methionine (M461 in the normal *ATP7A* sequence[2]) (**Figure 2a**). The total size of the AAV construct was 4.9 kb.

Since other evolutionary versions of this P-type ATPase contain copper-binding motifs ranging in number from one to six,[24] we anticipated that the *rsATP7A* allele with two N-terminal copper-binding sites would retain copper transport function. This was confirmed in yeast complementation assays, which indicated ~80% of normal copper transport capacity (**Figure 1c,d**). The $CuCl_2$ dose (50 ng total) was extrapolated from the maximum tolerated dose of intracerebroventricular copper histidine we previously determined in adult rats,[25] adjusted for differences in cerebrospinal fluid volume.

Mo-br males without treatment showed a mean survival of 13.3 ± 0.87 days, which was not significantly different than for affected mice treated with 10 µg/g body weight of intraperitoneal copper (**Figure 1f**). Lateral ventricle injections of AAV5-*rsATP7A* gene therapy alone, or copper alone each extended lifespan slightly ($P < 0.001$, and $P < 0.01$, respectively) but none survived to weaning (21 days) (**Figure 2c**). However, combining these two brain-directed treatments (AAV5+Cu) resulted in a large synergistic effect and rescue of *mo-br* males: 86% survived to weaning, median survival increased to 43 days, 37% lived beyond 100 days, and 22% survived to the study end point of 300 days ($P = 0.00001$, **Figure 2d**). Replacement of the *rsATP7A* transgene in AAV5 with green fluorescent protein (GFP) cDNA eliminated the rescue effect (**Figure 2d**, green circles).

Because of the natural history of untreated *mo-br* (death by 14 days of age), we sacrificed animals from each group at 12 days of age to analyze brain biochemistry and neuropathology. Brain copper levels in 12-day untreated mutants were less than 25% of wild type (**Figure 2e**). Brain-directed copper treatment alone increased brain copper slightly in the mutants, whereas AAV5+Cu treatment increased brain copper to ~50% of wild type ($P = 0.03$) (**Figure 2e**). Brain ratios of dihydroxyphenylacetic acid: dihydroxyphenylglycol (DOPAC: DHPG) (**Figure 2f**) were markedly increased in untreated *mo-br* mutants, reflecting dopamine-β-hydroxylase deficiency, similar to the neurochemical patterns in cerebrospinal fluid and plasma of infants with Menkes disease.[13,26] Neurochemical ratios in *mo-br* brain improved with both individual treatments, but were significantly different from the untreated mutant group only in response to AAV5+Cu ($P = 0.01$) (**Figure 2f**). In untreated *mo-br* mice, mean activity of brain cytochrome *c* oxidase (CCO), a mitochondrial cuproenzyme, was ~15% compared to wild type and increased to ~25% in all three treatment groups (**Figure 2g**). In contrast, the activity of Cu/Zn superoxide dismutase, a cytosolic enzyme, was ~80% of normal and treatment did not significantly enhance activity (**Supplementary Figure S1**), consistent with previous findings.[27]

Untreated *mo-br* mice showed scattered pyknotic neurons in the cerebral cortex and hippocampus at 12 days (**Figure 3a**). In a more detailed analysis (**Figure 3b**), we found a statistically significant higher percentage of abnormal pyknotic hippocampal neurons in untreated mutant mice ($P < 0.00001$) compared to wild type. The difference in abnormal neurons between AAV5+Cu combination-treated mice and the wild-type group was not statistically significant ($P = 0.07$). Diminished axonal development in the cerebral cortex, as measured by Bielschowsky silver staining, was also evident in 12 day untreated and, to a lesser extent, in the combination-treated mutant brains in 12-day untreated mutants (**Figure 3a**). Electron microscopy revealed swollen dendrites with fibrillar disorganization and pale mitochondria (**Figure 3a**). In contrast, 12-day AAV5+Cu combination-treated mutants displayed minimal ultrastructural pathology (**Figure 3a**).

Selective transduction of choroid plexus epithelia by AAV5-rsATP7A

To clarify the mechanism of the *mo-br* rescue, we assessed the expression pattern of *rsATP7A* in 12-day-old mice treated with AAV5. Despite inclusion in the cDNA of sequence for a 6x-His tag (**Figure 2a**), we did not detect the transgene protein in brain sections by immunohistochemical staining with anti-His antibodies, presumably due to cleavage of the 6x-His tag or inadequate assay sensitivity. Because Atp7a$^{mo\text{-}br}$ protein is not degraded[18] and high homology exists between human ATP7A and murine Atp7a[28], rsATP7A cannot be distinguished from Atp7a$^{mo\text{-}br}$ in immunohistochemical specimens with an anti-ATP7A antibody.[13] Instead, we evaluated the transduction pattern with the cDNA for GFP substituted for rsATP7A in our AAV5 construct. The treatment conditions

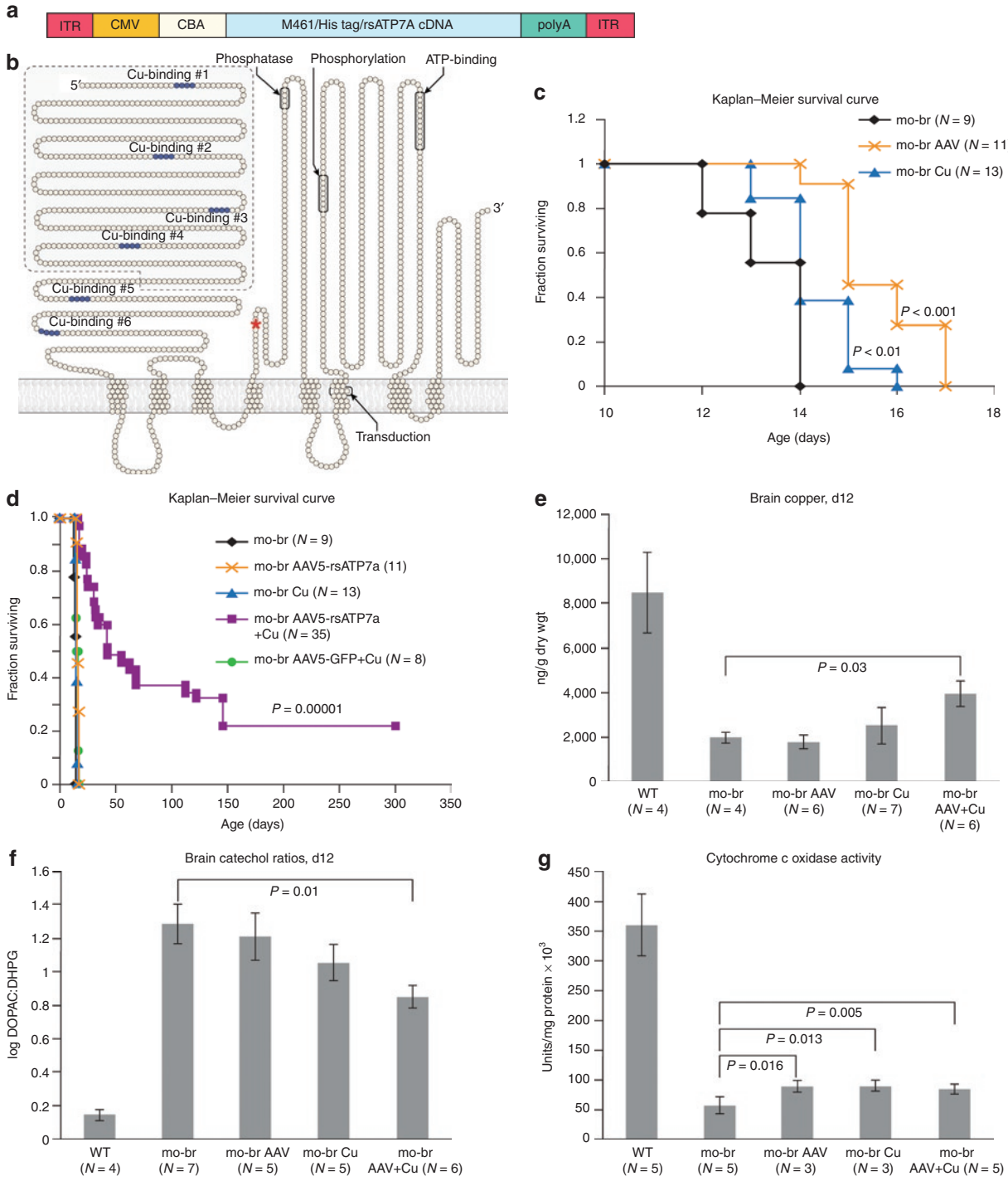

Figure 2 Brain-directed treatment strategy. (**a**) Elements of the adeno-associated virus serotype 5 (AAV5) construct. Flanked by inverted terminal repeat (ITR) motifs, the AAV5 construct includes a cytomegalovirus (CMV) enhancer, chicken β-actin (CBA) promotor, and complementary DNA (cDNA) for a reduced-size version (3.1 kb) of *ATP7A* (*rsATP7A*) beginning with amino acid residue 461, necessary due to AAV packaging size limit (~5 kb). The sequence for a 6x-His tag (CACCACCACCACCACCAC) was inserted immediately inside the ATG for methionine 461. The rabbit β-globin polyadenylation (polyA) signal terminates transcription. The entire AAV5-rsATP7A construct size was 4.9 kb. (**b**) Model of ATP7A with the shaded area indicating the segment removed, including the first four of six amino-terminal copper-binding sites, to generate *rsATP7A*. The red asterisk denotes location of the *mo-br* mutation (deletion of two conserved amino acids). (**c**) Kaplan–Meier survival curve indicating slight lengthening of lifespan with each individual brain-directed treatment. (**d**) Kaplan–Meier survival curve indicating synergy of intracerebroventricular AAV5+Cu therapy (lavender) in rescue of the *mo-br* mouse ($P = 0.00001$ compared to untreated *mo-br* mutants). Replacement of *rsATP7A* with *GFP* (green circles) eliminated the survival benefit. (**e**) Brain copper levels at 12 days of age, by treatment category. Only AAV5+Cu combination-treated *mo-br* mice showed significantly higher copper levels in comparison to untreated *mo-br* mice ($P < 0.03$). (**f**) Brain catechol ratios at 12 days of age, by treatment category. Only AAV5+Cu combination-treated *mo-br* mice showed significantly lower ratios, indicative of improved dopamine-β-hydroxylase activity ($P < 0.01$). (**g**) Brain cytochrome *c* oxidase activity at 12 days of age, by treatment category. All treatment groups showed significantly increased activity compared to untreated *mo-br* mice.

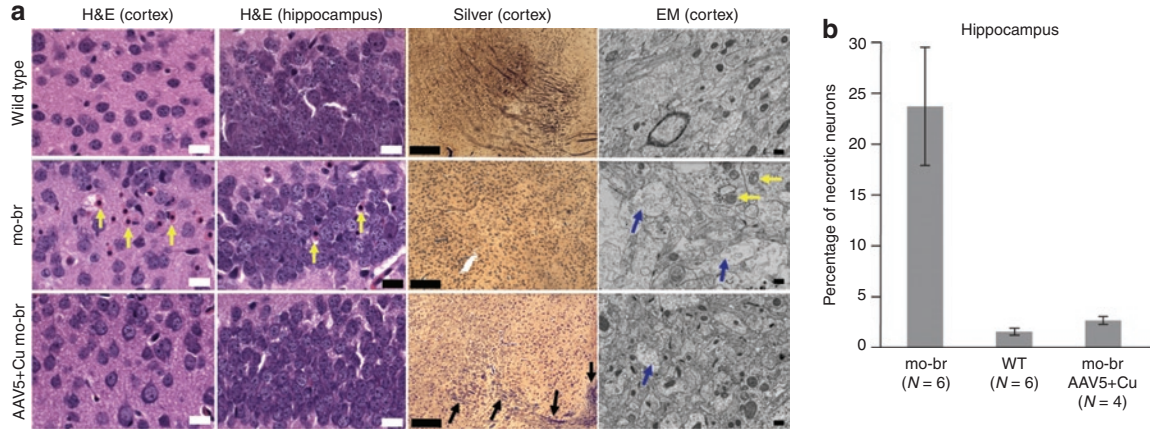

Figure 3 Brain pathology findings. (**a**) Twelve-day cerebral cortex and hippocampus in wild type, untreated *mo-br,* and combination-treated *mo-br* mice. Untreated mutants showed abnormal neurons with pyknotic nuclei (yellow arrows), which were not obvious in wild type or AAV5+Cu *mo-br* mice. Bielschowsky silver stain indicated minimal axonal development in untreated 12-day *mo-br* mice compared to wild type, whereas AAV5+Cu combination treatment was associated with early developing axons (arrows). Electron micrographs of untreated 12-day *mo-br* brain cortex showed palely stained mitochondria (yellow arrows) and swollen dendrites and reduced neurofilament density (blue arrows). The latter ultrastructural abnormality was also noted occasionally in the AAV5+Cu-treated 12-day *mo-br* mice. Scale bars indicate 25 µm in hematoxylin and eosin (H&E) panels, 200 µm in silver-stained slides, and 500 nm in electron micrographs. The images shown are representative of each treatment group based on pathologic analysis of at least four mice in each category. (**b**) Quantitation of abnormal pyknotic hippocampal neurons. Untreated *mo-br* mice show a markedly higher percentage of abnormal hippocampal neurons compared to wild type and AAV5+Cu combination-treated *mo-br* mice. Error bars reflect standard error of the mean. AAV5, adeno-associated virus serotype 5.

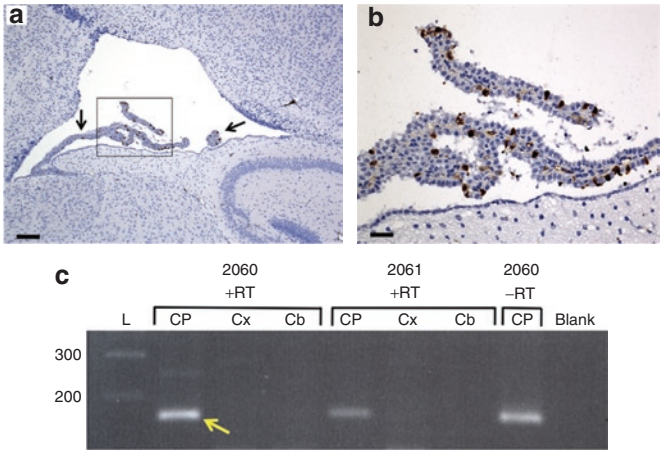

Figure 4 Selective transduction of choroid plexus epithelia. (**a**) Transduction of choroid plexus epithelia by AAV5-GFP. Low power (Scale bar = 160 µm) and (**c**) high power (Scale bar = 40 µm) views of the lateral ventricle and choroid plexus (arrow) from a 12-day-old wild type mouse brain stained with anti-GFP, to define the transduction pattern of AAV5 in these experiments. The same transduction pattern was evident in AAV5-GFP+Cu treated *mo-br* mice. (**b**) Reverse transcriptase (RT)-PCR and PCR confirm selective choroid plexus transduction by AAV5-rsATP7A. RT-PCR in mice 2,060 and 2,061 shows amplification of the 166 bp expected transgene product (yellow arrow) only in choroid plexus RNA samples. The transgene product was also detected in the choroid plexus RNA specimen from 2,060 without reverse transcription (lane 2,060 –RT).

remained identical. GFP was detectable in a small proportion of choroid plexus epithelial cells in the lateral ventricles using a polyclonal anti-GFP antibody (**Figure 4a,b**). These experiments demonstrated that AAV5 tropism was restricted to choroid plexus epithelia in wild type and *mo-br* mice, without discernible transduction of neurons or microglia (**Figure 4a**), as noted previously with intracerebroventricular administration of AAV5 by others.[29]

Using an established technique,[30] we also isolated choroid plexus tissue from the lateral ventricles of 12-day-old mice treated with AAV5-rsATP7A as newborns. We extracted total RNA from the choroid plexuses, as well as from cerebral cortex and cerebellum samples from these mice and performed reverse transcriptase (RT)-PCR to assess *rsATP7A* transgene expression. As expected, the RT-PCR product corresponding to the transgene was present only in choroid plexus samples (**Figure 4c**). The transgene PCR product was also detected in a choroid plexus RNA sample without RT (**Figure 4c**, lane 2060 –RT), consistent with retention of some AAV5-rsATP7A vector genomic DNA during RNA purification. In sum, these data confirmed selective transduction of the choroid plexus by AAV5-rsATP7A.

Long-term growth and neurobehavioral outcome of treatment

Weight gain in a subset (N = 12 at start) of AAV5+Cu-treated mutants paralleled but was slightly less robust than in normal littermates (**Figure 5a**). In a larger group (N = 19 at start) of AAV5+Cu-treated *mo-br* mice, we assessed neurobehavioral function. Beginning at age 25 days and up to 300 days, we performed weekly neurobehavioral phenotyping, using the wire hang test to evaluate neuromuscular strength and a constant speed rotarod test to measure balance and motor coordination (**Figure 5b,c**).

Since gross motor function is often impacted in Menkes disease patients,[13] we anticipated that motor delays in surviving *mo-br* mice were possible. Indeed, rescued mice performed less well than wild-type littermates on both tests (**Figure 5b,c**), although a trend toward improvement with age was evident, particularly on the wire hang test (**Figure 5b**). The transient decline in rotarod performance between 40 and 75 days of age (**Figure 5c**) may have reflected relative difficulty in adjusting to this test by rescued *mo-br* mutants during a rapid growth period (**Figure 5a**).

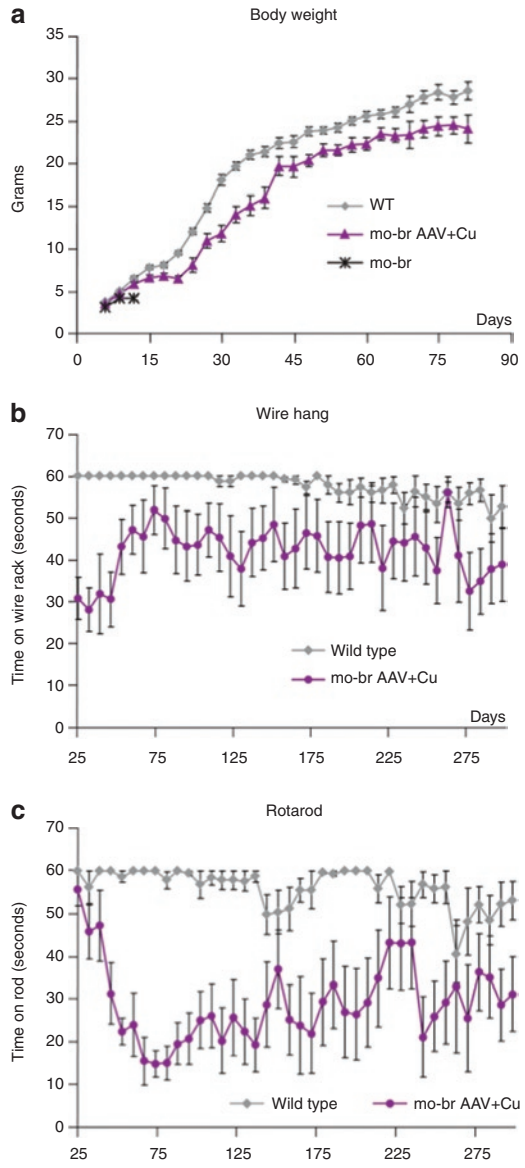

Figure 5 Long-term growth and neurobehavioral testing. (**a**) Weight gain in combination-treated *mo-br* mutants paralleled that for wild-type littermates (gray squares). (**b**) Wire hang and (**c**) rotarod test results. Tests were performed weekly beginning at 25 days of age, with three trials per time point, and used a 60 seconds maximum. AAV5, adeno-associated virus serotype 5.

We sought to correlate these functional deficits in balance and motor coordination with neuropathological effects in long-surviving *mo-br* mice. By 300 days, AAV5+Cu-treated mutants showed evidence of extensive myelination indistinguishable from wild type (**Figure 6a**) and there were minimal cortical ultrastructural abnormalities (**Figure 6b**). To evaluate effects in the cerebellum, a brain region particularly sensitive to copper deficiency,[6] we scored mitochondrial morphology in 107 Purkinje cells from electron micrographs of a 300-day AAV5+Cu-treated mutant and 265 Purkinje cells from two normal littermates. No increase in mitochondrial pathology was evident in the mutant animal (data not shown). However, evaluation of a larger number of 300-day old animals (six AAV5+Cu-treated *mo-br* and five wild-type controls) with routine hematoxylin and eosin staining of brain sections suggested increased Purkinje cell loss in the mutant animals (**Figure 6c**). Because Purkinje cells are crucial for motor coordination, these latter findings could be highly relevant to the rescued animals' suboptimal performance on the rotarod.

DISCUSSION

Our results provide mechanistic insights concerning efficacious brain-directed treatment of a mouse model for Menkes disease, a lethal genetic disorder of copper metabolism. Whereas both individual brain-directed treatments extended *mo-br* lifespan slightly (**Figure 2c**) and improved neurotransmitter ratios modestly (**Figure 2f**), only copper treatment increased brain copper levels (**Figure 2e**). These cumulative results suggested that the two therapies had different effects: copper injections increasing total copper available to the brain, and AAV5 gene therapy improving copper utilization. We hypothesized that combining the two therapies would yield a synergistic effect. Indeed, combination therapy dramatically enhanced survival, as demonstrated in the AAV5+Cu treatment group (**Figure 2d**).

This study represents the first application of gene therapy for Menkes disease. This neurometabolic condition might be considered an unlikely candidate for gene therapy because ATP7A is a large transmembrane protein, expressed ubiquitously, and not secreted. However, our data in *mo-br* mice suggest that bolstering copper transport activity at the blood–cerebrospinal fluid barrier, together with repletion of cerebrospinal fluid copper, is sufficient for vastly improved outcomes. The trend toward improvement in tests of neuromuscular strength and balance observed as rescued mice became older (**Figure 5b,c**) suggests that AAV5+Cu provided the potential for near normal, albeit delayed, neurologic maturation in some *mo-br* mice.

Our findings also advance the concept that choroid plexus epithelia are critically important for central nervous system copper homeostasis, and highlight the possibility that these cells, which form the blood–cerebrospinal fluid barrier, represent a useful therapeutic avenue for amelioration of other inherited neurometabolic diseases. Restriction of AAV5 transduction to the choroid plexus epithelia (**Figure 4**) is consistent with previous evaluation of the AAV5 transduction profile after lateral ventricle injection.[29] In the present context, this finding implies that the *mo-br* rescue results from improved copper retention in cerebrospinal fluid and brain (**Figure 2e**) by expression of rsATP7A in these polarized cells. Western blots of choroid plexus tissue to detect rsATP7A protein proved difficult to interpret due to persistent high background staining in the molecular mass range expected for the transgene product.

Choroid plexus epithelia have a very slow turnover rate compared to other slow-renewing epithelia;[31] under normal conditions, choroid plexus epithelia are not replaced in the mouse adult life span. Thus, these nonreplicating cells are ideal targets for a nonintegrating, episomal AAV vector capable of sustaining long-term transgene expression.[32]

Polarized choroid plexus epithelia project their apical surfaces into cerebrospinal fluid contained within the four intracerebral ventricles, with the basolateral membranes adjoining the underlying vasculature.[33] Prior studies have confirmed robust *Atp7a*

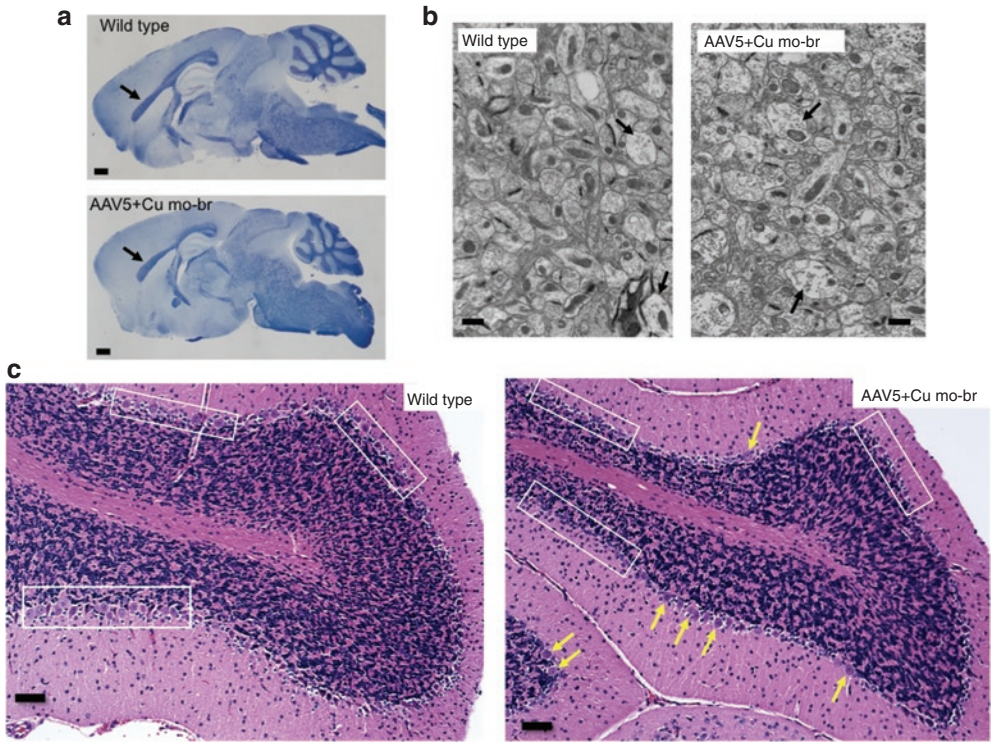

Figure 6 Neuropathology in 300-day wild type and AAV5+Cu-treated mo-br mice. (**a**) Luxol fast blue staining for myelin indicated the expected dense myelination of the corpus callosum (arrows) in sagittal brain sections from 300-day wild type and AAV5+Cu-treated mutants. Bar = 1 mm. (**b**) At 300 days of age, electron micrographs of brain cortex showed minimal differences between an AAV5+Cu-treated *mo-br* mutant and a normal littermate control. The combination-treated brains contained some dendrites with reduced neurofilament density and less organized architecture (arrows), although 300-day wild-type brain also showed occasional dendrites with similar abnormalities (arrow). Three animal pairs were examined, with representative results shown. Bar = 500 nm. (**c**) Cerebellar histopathology in wild type and 300-day AAV5+Cu-treated *mo-br* animals indicated subtle differences in the Purkinje cell layer of the treated mutants. While many normal Purkinje neurons (yellow arrows) were visible in *mo-br* mice, some regions of the Purkinje cell layer (boxed areas) showed few or no Purkinje neurons compared to wild type (boxed areas). These differences may be relevant to *mo-br* rotarod performance. Bar = 50 µm. AAV5, adeno-associated virus serotype 5.

expression in these cells.[34–36] Although ATP7A localizes to the basolateral surfaces after copper loading in most polarized cells,[8,37] we predict a reversal of copper ATPase sorting in choroid plexus epithelia with resultant apical localization of ATP7A.[5] There is a precedent for this phenomenon; Na^+/K^+ ATPase localizes to the apical rather than the basolateral membrane of the choroid plexus epithelia.[38,39] All other polarized cells express Na^+/K^+ ATPase basolaterally. In addition, some cytoskeleton components exhibit reversed polarity in choroid plexus epithelia.[39] Furthermore, study of tissues and cerebrospinal fluid from a patient with *ATP7A* somatic mosaicism strongly suggested that choroid plexus epithelia mediate copper delivery to, rather than exodus from, the developing human brain.[7] Finally, the choroid plexus has been shown to regulate brain uptake of manganese, indicating its crucial role in central nervous system delivery of another paramagnetic transition metal.[40]

We postulate that copper utilization for axon and synapse development, neuronal activation, and metallation of cuproenzymes in these mice was enabled by $Atp7a^{mo\text{-}br}$ residual activity, improved delivery of brain copper by neuronal copper chaperones, or via *Atp7b*, a closely related copper transporter.[5] The capacity for complementarity between ATP7A and ATP7B in the central nervous system remains obscure[37] and represents an important topic for future study.

The brain catechol ratio results (**Figures 2f**) suggest that dopamine-β-hydroxylase and other copper enzymes processed in the *trans*-Golgi compartment, such as peptidylglycine-α-amidating monooxygenase, can be metallated in *mo-br* brain if sufficient copper is available. The cytosolic copper chaperone ATOX1 ferries copper to both ATP7A and ATP7B at the *trans*-Golgi membrane, their default intracellular location. When metallated, peptidylglycine-α-amidating monooxygenase removes the carboxy-terminal glycine residues of numerous neuroendocrine peptide precursors (*e.g.*, gastrin, cholecystokinin, vasoactive intestinal peptide, corticotropin-releasing hormone, thyrotropin-releasing hormone, calcitonin, vasopressin, neuropeptide Y, pituitary adenylyl cyclase-activating polypeptide), and is required for neurogenesis and neuronal survival.[41]

In contrast to dopamine-β-hydroxylase, we did not observe a clear synergistic effect of AAV5 gene therapy and copper treatment in terms of CCO activity (**Figure 2g**). While the statistical *P* value was most significant for AAV5+Cu, each of the individual treatments significantly increased activity of this mitochondrial copper enzyme in comparison to untreated controls (**Figure 2g**). The reason for increased CCO activity with AAV5 treatment alone remains unclear, because rsATP7A is not expected to participate in copper delivery to the mitochondria, and also because we found no evidence of neuronal transduction.

The relatively low viral titer (2.5×10^8) required for the success described in these experiments is encouraging and also potentially explains the incomplete correction of *mo-br*. We suspect that minor differences in choroid plexus transduction efficiency may have contributed to the variable life spans noted. Thus, follow-up studies to evaluate further improvements in survival and neurological outcomes using higher AAV5 concentrations will be informative. Because the copper dose employed was based on the maximum tolerated dose in adult rats,[25] this parameter is less adjustable. Use of helper-dependent adenovirus as a brain-directed gene transfer vector could also improve outcomes, given its large cloning capacity (up to 37 kb) which would allow transfer of the full-length human ATP7A, as well as its capacity for choroid plexus transduction.[42]

The prospect of clinical gene therapy to ameliorate devastating inherited neurometabolic diseases has intuitive appeal, although concerns regarding the risk: benefit ratio of this approach remain. Gene therapy with AAVs has already been employed in clinical trials for human neurological disorders, including Parkinson's disease, late infantile neuronal ceroid lipofuscinosis, Leber's congenital amaurosis, and type 2D limb-girdle muscular dystrophy.[43–46] Based on the disease requirement, either brain-, retina-, or muscle-directed approaches were applied. For future clinical applications in Menkes disease, gene therapy that targets choroid plexus epithelia theoretically could be accomplished via a single intrathecal injection. In cases of *ATP7A* mutations previously documented in Menkes disease patients who did not respond optimally to early copper injection treatment,[6,13,14] the potential clinical benefits of brain-directed gene therapy may outweigh the potential risks.[47]

Our findings provide initial evidence that gene therapy may have clinical utility in the treatment of human patients with Menkes disease. AAV vectors with different serotypes such as AAV9 or AAVRh10, which show broader neuronal tropism than AAV5 and may gain access to the brain after peripheral administration[47,48] could prove particularly suitable for this purpose. Further preclinical studies to address these questions are warranted.

MATERIALS AND METHODS

Mice. C57BL/6-*Atp7a*$^{mo\text{-}br}$ breeding pairs were obtained from Jackson Laboratories (Bar Harbor, ME). Each breeding pair consisted of a female heterozygous for the *Atp7a*$^{mo\text{-}br}$ allele and a wild-type male. After the first generation, breeding pairs consisted mainly of sib crosses. For experiments, litters were culled to 4–5 pups. Shortly after birth, toe biopsies were performed for genotyping and later identification. Genomic DNA was isolated and the region containing the *mo-br* 6 bp deletion was amplified with primers *mo-br* forward, 5′-AAC ACT TTC TTT CTT CAG CAC-3′, and *mo-br* reverse, 5′-TGC TTG TAA TGA AAT TAG CTT GG-3′. PCR conditions were as follows: 94° for 5 minutes (1 cycle); 94° for 30 seconds, 60° for 30 seconds, 72° for 30 seconds (35 cycles), and 72° for 7 minutes final extension. The PCR product was digested with *HaeIII* and electrophoresed though a 2.5% agarose gel. All experimental procedures were approved by the NICHD Animal Studies Committee.

Yeast complementation assays. The respective cDNA constructs were generated and cloned into pYES plasmids which were used to transform the *S. cerevisiae* copper transport mutant, *ccc2*Δ, as previously described.[13] Transformed or mock-transformed strains were cultured in copper-limited solid or liquid media and experiments were performed in triplicate.

HEK-293T cell transfection. Full-length *Atp7A* cDNA was constructed by RT-PCR using total RNA from wild-type mouse brain as template to generate three overlapping fragments. Site-directed mutagenesis was used to generate the *Atp7a*$^{mo\text{-}br}$ allele, a deletion of six bases encoding amino acids 799 (Ala) and 800 (Leu). After sequence fidelity was confirmed, the cDNAs were inserted between the *Sac*I and *Apa*I sites of pEYFP-C1 plasmids and used, individually, for transfection of HEK-293T cells. Cells were viewed by a confocal microscope (Zeiss 510; Carl Zeiss Microimaging, LLC, Thornwood, NY) and images captured using META software. The transfections were performed in duplicate and ~1,000 wildtype- and *Atp7A*$^{mo\text{-}br}$-transfected cells were examined. DAPI nuclear counterstain (Electron Microscopy Sciences, Fort Washington, PA) and an anti-TGN46 antibody (Novus Biologicals, Littleton, CO) were used according to the manufacturers' instructions.

Western blot. Protein was isolated from the brains of wild type and untreated *mo-br* mice and denatured by adding 5× loading buffer with 5% β-mercaptoethanol (Quality Biological, Gaithersburg, MD), and heating at 50 °C for 10 minutes. Samples (40 µg total protein) were electrophoresed through 4–12% NOVEX Tris–Glycerin SDS-polyacrylamide (Invitrogen, Carlsbad, CA), and transferred to polyvinylidene fluoride membranes. Membranes were incubated at 4 °C overnight in Tris-buffered saline blocking buffer [0.9% (vol/vol) NaCl, 20 mmol/l Tris/HCl, pH 7.5, 0.5% SDS (vol/vol), 0.1% Tween 20 (vol/vol)] containing 5% (wt/vol) nonfat milk. Blots were washed with Tris-buffered saline, then incubated for 3 hours with a 1:1,000 dilution of a rabbit anti-ATP7A antibody raised against the carboxy-terminal 18 amino acids (NH2-DKHSLLVGDFREDDDTAL-OH) of human ATP7A (Antibody Solutions, Sunnyvale, CA). After washing, membranes were incubated with anti-rabbit IgG horseradish peroxidase conjugate (1:2,000; Santa Cruz Biotechnology, Santa Cruz, CA) for 1 hour at room temperature, washed, and developed using SuperSignal West Pico Luminol/Enhancer Solution (Pierce, Rockford, IL), according to the manufacturer's instructions. After membrane stripping, β-actin was detected by blocking with a primary mouse anti-β-actin monoclonal antibody conjugated with horseradish peroxidase (Santa Cruz Biotechnology) and developed using an enhanced chemiluminescence reagent, as above.

Intraperitoneal copper injections. Six *mo-br* male mice received a single intraperitoneal injection of $CuCl_2$ at a dose of 10 µg/g body weight (~50 µg) on day 7 of life, as previously described.[21,22]

rAAV5-rsATP7A. A reduced-size human ATP7A cDNA (*rsATP7A*), was amplified by from pAD-LOX-GFP-MNK (gift of Ann Hubbard) using primers 5′GAGCCATGGACCACCATGCATCATCACCACCATCACCC GCTTTTGACTTCAACTAAT-3′ (forward), and 5′-GAGAGCCCGGG CGGCCGCGAATTCGAGCTCGGTACCCG-3′ (reverse), and cloned into pTR-CAGGS-Enh (gift of Mark Sands), downstream of the chicken β-actin promoter. Large scale production of plasmid was performed using an Endo-free Plasmid Mega Kit (Qiagen, Valencia, CA). To produce rAAV5, HEK-293T cells were transfected with the calcium phosphate method. Briefly, three plasmids were co-transfected in a 1:1:2 ratio: the rAAV plasmid, MMTV5, and pRS449b. Cells were harvested at 72 hours, lysed by free-thawing, and the lysate fractionated by CsCl centrifugation. Fractions (500 µl) were assayed for viral content by quantitative PCR with primers 5′-CACCAGTTCAAGACAAGGAGG-3′ and 5′-CTTACTTCTGCCTTG CCAGC-3′. The virus-containing fractions were pooled, concentrated, and dialyzed against lactated Ringer's solution. Final virus concentration was determined by real-time quantitative PCR on a MJ Research DNA Engine Opticon instrument.

Intracerebroventricular injections. Injections were performed with a 5 µl Hamilton syringe fitted with a custom needle (32 gauge, 9.5 mm long, point 4) on day two or three of life. Lateral ventricle delivery with this technique was confirmed in several animals by injection of 2% toluidine blue solution (data not shown). $CuCl_2$ in a total dose of 50 ng

(extrapolated from the maximum tolerated dose of copper in adult rats[25] and adjusted for differences in cerebrospinal fluid volume) was administered. $CuCl_2$ was diluted in 10 mmol/l Tris, 150 mmol/l NaCl, pH 7.5 to a final concentration of 6.25 ng/μl. Four microliters were injected bilaterally a depth of 2.5 mm. Injections were administered at a point 2.5 mm anterior to bregma and 2.0 mm lateral to the midline. For rAAV5 injections, 2 μl of virus (1.25×10^8 viral particles/μl) in lactated Ringer's was injected bilaterally. For mice receiving AAV5+Cu, the AAV5 injections were performed on day two of life and the copper injections were performed on day three of life.

Brain copper measurement. Copper levels in fresh frozen brains were determined by graphite furnace atomic absorption and confirmed by inductively coupled plasma mass spectrometry, as previously described.[25]

Brain neurochemical levels. Half of each brain was weighed and immediately homogenized in 5–10 volumes of 0.4 N perchloric acid containing 0.1% ethylene diamine tetra-acetic acid. The homogenates were centrifuged and supernatant frozen at −70 °C until assay. Concentrations of brain neurochemicals dihydroxyphenylacetic acid and dihydroxyphenylglycol were determined by high-performance liquid chromatography with electrochemical detection.

Copper enzyme assays. CCO and SOD1 assays were performed as previously described.[49]

Pathology. Mice were killed with CO_2 gas, and brains were promptly removed. One hemisphere of each brain was fixed in 10% neutral buffered formalin. Paraffin embedding was performed by Histoserve (Germantown, MD). Sections (5–15 micron thickness) were stained with hemotoxylin and eosin, Bielschowsky silver stain, or Luxol fast blue.

For electron microscopy, deep anesthesia was achieved with pentobarbital in saline, and mice were perfused with phosphate-buffered saline, followed by 4% paraformaldehyde in phosphate-buffered saline (pH 7.2) before brain removal. Brains were fixed with 2% OsO_4 in cacodylate buffer for 2 hours, washed with 0.1 mol/l cacodylate buffer three times, washed with water, and placed in 1% uranyl acetate for 1 hour. Brains were then serially dehydrated in ethanol and propylene oxide, and embedded in EMBed 812 resin (Electron Microscopy Sciences). Thin sections (~80 nm) from frontal cortex or cerebellum were obtained with the Leica ultracut-UCT ultramicrotome (Leica, Deerfield, IL), placed onto 300 mesh grids, and stained with saturated uranyl acetate in 50% methanol and then with lead citrate. Grids were viewed in a JEM-1200EXII electron microscope (JEOL, Tokyo, Japan) at 80 kV and images were recorded on the XR611-M mid-mounted 10.5 megapixel CCD camera (Advanced Microscopy Techniques, Danvers, MA). We examined 75–100 electron micrograph images per treatment group and brain region.

Quantitation of hippocampal neuronal cell death. From hematoxylin and eosin stained sagittal brain sections, 400–600 hippocampal neurons per animal were scored as either normal or necrotic (defined as hypereosinophilic with pyknotic nuclei) in 12 day mice from three groups: untreated mo-br ($N = 6$), wild type ($N = 6$), and AAV5+Cu-treated *mo-br*. The mean percentage of necrotic neurons was calculated for each group and evaluated for statistically significant differences via the Student's *t*-test.

Mitochondrial architecture scoring. Mitochondrial architecture was assessed in ~400 mitochondria from electron micrographs of selected Purkinje cell neurons. The mitochondria were scored blindly based on the following scheme: 1 = no vacuolization; 2 = mild-moderate vacuolization; 3 = moderate-severe vacuolization.

GFP immunohistochemistry. Tissues were rehydrated, and antigen retrieved with citrate buffer, pH 6.0 for 20 minutes in a steamer and allowed to cool to room temperature. The slides were subsequently rinsed with Tris-buffered saline Tween 20 distilled H_2O used for the final rinse. All tissues were treated with dual endogenous block (DAKO, Carpinteria, CA) two times for 5 minutes and subsequently protein blocked for 5 minutes before the application of the primary antibody. Tissue was incubated with GFP clone JL-8 for 1 hour (1:2,000; Clontech, Mountain View, CA). The slides were then washed twice with Tris-buffered saline and Tween 20, incubated with DAKO EnVision mouse peroxidase for 30 minutes, followed by DAB^+ for 10 minutes. (DAKO) and counterstained with hematoxylin. For a negative control, the primary antibody was replaced with mouse IgGs at the same concentration.

Choroid plexus isolation. Choroid plexuses were isolated from the lateral ventricles of 12-day-old AAV5-treated and untreated mice, following procedures described by Menheniott *et al.*[30]

RT-PCR. Total RNA in brain samples from AAV5-treated and untreated mice was extracted using RNeasy Lipid Tissue Mini Kit (Qiagen). First strand cDNA synthesis was performed using Enhanced Avian TR First Strand Synthesis Kit (Sigma, St Louis, MO). PCR to detect a 166 bp *rsATP7A* transgene fragment was performed using primers (forward: 5′-CACCAGTTCAAGAC AAGGAGG-3′; and reverse 5′-CTTACTTCTGCCTTGCCAGC-3′). PCR products were analyzed on a 2.5% agarose gel.

Statistical analyses. One-way analysis of variance analysis was used to evaluate CCO and SOD1 enzyme activity. We assessed whether any *mo-br* group, treated or untreated, was different than the wild-type group using Dunnett's test. Brain copper and neurochemical data and hippocampal neuron data were analyzed by paired Student's *t*-tests.

Neurobehavioral testing. Wild-type and AAV5+Cu-treated *mo-br* mice were tested repeatedly using two neurobehavioral tests (wire hand, rotarod) to evaluate muscle strength, balance, coordination, and locomotor function. Testing was performed weekly beginning at 25 days of age and until the mice reached 300 days or expired. Nineteen AAV5+Cu-treated *mo-br* mice and 11 untreated wild-type controls were tested. Untreated *mo-br* mice were unavailable for testing because these mice all died before weaning.

The wire hang test was performed as described previously.[50] Briefly, mice were placed on a wire cage rack 50 cm above a soft surface. The rack was inverted and the length of time the mouse could hang from the rack was measured (maximum time: 60 seconds). The test was repeated up to three times with at least 1 minute of rest in between trials if the animal failed to complete the full 60 seconds, and the time scored was the maximum of the three trials.

The constant speed rotarod was performed as described previously.[50] Briefly, mice were placed on a 3.5 cm diameter rod (IITC, Woodland Hills, CA). The rod was rotated at 4 r.p.m. and the length of time the mouse could remain on the rod was measured (maximum time: 60 seconds). The test was repeated up to three times with at least 1 minute between trials if the animal failed to complete the full 60 seconds. The time scored was the maximum of the three trials. The mice were acclimated to the rod for four consecutive days (from 21 to 24 days) before testing beginning at 25 days.

SUPPLEMENTARY MATERIAL

Figure S1. Brain Cu/Zn superoxide dismutase activity at 12 days of age, by treatment category.

ACKNOWLEDGMENTS

We thank Jingrong Tang, Simina Lal, Hanna Xu, Margaret Broderius, Hayden Ollivierre-Wilson for technical assistance, and the NICHD Microscopy & Imaging Core and the NINDS DNA Sequencing Facility. This work was supported by the Intramural Research Program of the US National Institutes of Health. This work was performed in Bethesda, MD, USA.

REFERENCES

1. Menkes, JH, Alter, M, Steigleder, GK, Weakley, DR and Sung, JH (1962). A sex-linked recessive disorder with retardation of growth, peculiar hair, and focal cerebral and cerebellar degeneration. *Pediatrics* **29**: 764–779.
2. Vulpe, C, Levinson, B, Whitney, S, Packman, S and Gitschier, J (1993). Isolation of a candidate gene for Menkes disease and evidence that it encodes a copper-transporting ATPase. *Nat Genet* **3**: 7–13.
3. Chelly, J, Tümer, Z, Tønnesen, T, Petterson, A, Ishikawa-Brush, Y, Tommerup, N *et al.* (1993). Isolation of a candidate gene for Menkes disease that encodes a potential heavy metal binding protein. *Nat Genet* **3**: 14–19.
4. Mercer, JF, Livingston, J, Hall, B, Paynter, JA, Begy, C, Chandrasekharappa, S *et al.* (1993). Isolation of a partial candidate gene for Menkes disease by positional cloning. *Nat Genet* **3**: 20–25.
5. Kaler, SG (2011). ATP7A-related copper transport diseases-emerging concepts and future trends. *Nat Rev Neurol* **7**: 15–29.
6. Liu, PC, Chen, YW, Centeno, JA, Quezado, M, Lem, K and Kaler, SG (2005). Downregulation of myelination, energy, and translational genes in Menkes disease brain. *Mol Genet Metab* **85**: 291–300.
7. Donsante, A, Johnson, P, Jansen, LA and Kaler, SG (2010). Somatic mosaicism in Menkes disease suggests choroid plexus-mediated copper transport to the developing brain. *Am J Med Genet A* **152A**: 2529–2534.
8. Petris, MJ, Mercer, JF, Culvenor, JG, Lockhart, P, Gleeson, PA and Camakaris, J (1996). Ligand-regulated transport of the Menkes copper P-type ATPase efflux pump from the Golgi apparatus to the plasma membrane: a novel mechanism of regulated trafficking. *EMBO J* **15**: 6084–6095.
9. El Meskini, R, Cline, LB, Eipper, BA and Ronnett, GV (2005). The developmentally regulated expression of Menkes protein ATP7A suggests a role in axon extension and synaptogenesis. *Dev Neurosci* **27**: 333–348.
10. Schlief, ML, Craig, AM and Gitlin, JD (2005). NMDA receptor activation mediates copper homeostasis in hippocampal neurons. *J Neurosci* **25**: 239–246.
11. Schlief, ML, West, T, Craig, AM, Holtzman, DM and Gitlin, JD (2006). Role of the Menkes copper-transporting ATPase in NMDA receptor-mediated neuronal toxicity. *Proc Natl Acad Sci USA* **103**: 14919–14924.
12. El Meskini, R, Crabtree, KL, Cline, LB, Mains, RE, Eipper, BA and Ronnett, GV (2007). ATP7A (Menkes protein) functions in axonal targeting and synaptogenesis. *Mol Cell Neurosci* **34**: 409–421.
13. Kaler, SG, Holmes, CS, Goldstein, DS, Tang, J, Godwin, SC, Donsante, A *et al.* (2008). Neonatal diagnosis and treatment of Menkes disease. *N Engl J Med* **358**: 605–614.
14. Kaler, SG, Liew, CJ, Donsante, A, Hicks, JD, Sato, S and Greenfield, JC (2010). Molecular correlates of epilepsy in early diagnosed and treated Menkes disease. *J Inherit Metab Dis* **33**: 583–589.
15. Kaler, SG, Gallo, LK, Proud, VK, Percy, AK, Mark, Y, Segal, NA *et al.* (1994). Occipital horn syndrome and a mild Menkes phenotype associated with splice site mutations at the MNK locus. *Nat Genet* **8**: 195–202.
16. Kennerson, ML, Nicholson, GA, Kaler, SG, Kowalski, B, Mercer, JF, Tang, J *et al.* (2010). Missense mutations in the copper transporter gene ATP7A cause X-linked distal hereditary motor neuropathy. *Am J Hum Genet* **86**: 343–352.
17. Reed, V and Boyd, Y (1997). Mutation analysis provides additional proof that mottled is the mouse homologue of Menkes' disease. *Hum Mol Genet* **6**: 417–423.
18. La Fontaine, S, Firth, SD, Lockhart, PJ, Brooks, H, Camakaris, J and Mercer, JF (1999). Intracellular localization and loss of copper responsiveness of Mnk, the murine homologue of the Menkes protein, in cells from blotchy (Mo blo) and brindled (Mo br) mouse mutants. *Hum Mol Genet* **8**: 1069–1075.
19. Hunt, DM (1974). Primary defect in copper transport underlies mottled mutants in the mouse. *Nature* **249**: 852–854.
20. Hunt, DM (1976). A study of copper treatment and tissue copper levels in the murine congenital copper deficiency, mottled. *Life Sci* **19**: 1913–1919.
21. Mann, JR, Camakaris, J, Danks, DM and Walliczek, EG (1979). Copper metabolism in mottled mouse mutants: copper therapy of brindled (Mobr) mice. *Biochem J* **180**: 605–612.
22. Nagara, H, Yajima, K and Suzuki, K (1981). The effect of copper supplementation on the brindled mouse: a clinico-pathological study. *J Neuropathol Exp Neurol* **40**: 428–446.
23. Doetschman, T (2009). Influence of genetic background on genetically engineered mouse phenotypes. *Methods Mol Biol* **530**: 423–433.
24. Lutsenko, S and Kaplan, JH (1995). Organization of P-type ATPases: significance of structural diversity. *Biochemistry* **34**: 15607–15613.
25. Lem, KE, Brinster, LR, Tjurmina, O, Lizak, M, Lal, S, Centeno, JA *et al.* (2007). Safety of intracerebroventricular copper histidine in adult rats. *Mol Genet Metab* **91**: 30–36.
26. Kaler, SG, Goldstein, DS, Holmes, C, Salerno, JA and Gahl, WA (1993). Plasma and cerebrospinal fluid neurochemical pattern in Menkes disease. *Ann Neurol* **33**: 171–175.
27. Phillips, M, Camakaris, J and Danks, DM (1986). Comparisons of copper deficiency states in the murine mutants blotchy and brindled. Changes in copper-dependent enzyme activity in 13-day-old mice. *Biochem J* **238**: 177–183.
28. Levinson, B, Vulpe, C, Elder, B, Martin, C, Verley, F, Packman, S *et al.* (1994). The mottled gene is the mouse homologue of the Menkes disease gene. *Nat Genet* **6**: 369–373.
29. Watson, DJ, Passini, MA and Wolfe, JH (2005). Transduction of the choroid plexus and ependyma in neonatal mouse brain by vesicular stomatitis virus glycoprotein-pseudotyped lentivirus and adeno-associated virus type 5 vectors. *Hum Gene Ther* **16**: 49–56.
30. Menheniott, TR, Charalambous, M and Ward, A (2010). Derivation of primary choroid plexus epithelial cells from the mouse. *Methods Mol Biol* **633**: 207–220.
31. McDonald, TF and Green, K (1988). Cell turnover in ciliary epithelium compared to other slow renewing epithelia in the adult mouse. *Curr Eye Res* **7**: 247–252.
32. Brunetti-Pierri, N and Auricchio A (2010) Gene Therapy of Human Inherited Diseases. In The Online Metabolic and Molecular Basis of Inherited Disease, <http://www.ommbid.com//OMMBID/the_online_metabolic_and_molecular_bases_of_inherited_disease/b/abstract/part2/ch5.2>.
33. Wolburg, H and Paulus, W (2010). Choroid plexus: biology and pathology. *Acta Neuropathol* **119**: 75–88.
34. Kuo, YM, Gitschier, J and Packman, S (1997). Developmental expression of the mouse mottled and toxic milk genes suggests distinct functions for the Menkes and Wilson disease copper transporters. *Hum Mol Genet* **6**: 1043–1049.
35. Niciu, MJ, Ma, XM, El Meskini, R, Ronnett, GV, Mains, RE and Eipper, BA (2006). Developmental changes in the expression of ATP7A during a critical period in postnatal neurodevelopment. *Neuroscience* **139**: 947–964.
36. Choi, BS and Zheng, W (2009). Copper transport to the brain by the blood-brain barrier and blood-CSF barrier. *Brain Res* **1248**: 14–21.
37. Barnes, N, Bartee, MY, Braiterman, L, Gupta, A, Ustiyan, V, Zuzel, V *et al.* (2009). Cell-specific trafficking suggests a new role for renal ATP7B in the intracellular copper storage. *Traffic* **10**: 767–779.
38. Quinton, PM, Wright, EM and Tormey, JM (1973). Localization of sodium pumps in the choroid plexus epithelium. *J Cell Biol* **58**: 724–730.
39. Alper, SL, Stuart-Tilley, A, Simmons, CF, Brown, D and Drenckhahn, D (1994). The fodrin-ankyrin cytoskeleton of choroid plexus preferentially colocalizes with apical Na+K(+)-ATPase rather than with basolateral anion exchanger AE2. *J Clin Invest* **93**: 1430–1438.
40. Aoki, I, Wu, YJ, Silva, AC, Lynch, RM and Koretsky, AP (2004). *In vivo* detection of neuroarchitecture in the rodent brain using manganese-enhanced MRI. *Neuroimage* **22**: 1046–1059.
41. Hansel, DE, May, V, Eipper, BA and Ronnett, GV (2001). Pituitary adenylyl cyclase-activating peptides and α-amidation in olfactory neurogenesis and neuronal survival in vitro. *J Neurosci* **21**: 4625–4636.
42. Dindot, S, Piccolo, P, Grove, N, Palmer, D and Brunetti-Pierri, N (2011). Intrathecal injection of helper-dependent adenoviral vectors results in long-term transgene expression in neuroependymal cells and neurons. *Hum Gene Ther* **22**: 745–751.
43. Kaplitt, MG, Feigin, A, Tang, C, Fitzsimons, HL, Mattis, P, Lawlor, PA *et al.* (2007). Safety and tolerability of gene therapy with an adeno-associated virus (AAV) borne GAD gene for Parkinson's disease: an open label, phase I trial. *Lancet* **369**: 2097–2105.
44. Maguire, AM, Simonelli, F, Pierce, EA, Pugh, EN Jr, Mingozzi, F, Bennicelli, J *et al.* (2008). Safety and efficacy of gene transfer for Leber's congenital amaurosis. *N Engl J Med* **358**: 2240–2248.
45. Worgall, S, Sondhi, D, Hackett, NR, Kosofsky, B, Kekatpure, MV, Neyzi, N *et al.* (2008). Treatment of late infantile neuronal ceroid lipofuscinosis by CNS administration of a serotype 2 adeno-associated virus expressing CLN2 cDNA. *Hum Gene Ther* **19**: 463–474.
46. Mendell, JR, Rodino-Klapac, LR, Rosales, XQ, Coley, BD, Galloway, G, Lewis, S *et al.* (2010). Sustained α-sarcoglycan gene expression after gene transfer in limb-girdle muscular dystrophy, type 2D. *Ann Neurol* **68**: 629–638.
47. Breakefield, XO and Sena-Esteves, M (2010). Healing genes in the nervous system. *Neuron* **68**: 178–181.
48. Hu, C, Busuttil, RW and Lipshutz, GS (2010). RH10 provides superior transgene expression in mice when compared with natural AAV serotypes for neonatal gene therapy. *J Gene Med* **12**: 766–778.
49. Prohaska, JR (1991). Changes in Cu,Zn-superoxide dismutase, cytochrome c oxidase, glutathione peroxidase and glutathione transferase activities in copper-deficient mice and rats. *J Nutr* **121**: 355–363.
50. Karl, T, Pabst, R and von Hörsten, S (2003). Behavioral phenotyping of mice in pharmacological and toxicological research. *Exp Toxicol Pathol* **55**: 69–83.